Phosphorylation and nuclear transit modulate the balance between normal function and terminal aggregation of the yeast RNA-binding protein Ssd1

Cornelia Kurischko[†,*] and James R. Broach
Department of Biochemistry, Penn State University College of Medicine, Hershey, PA 17033

ABSTRACT **Yeast Ssd1 is an RNA-binding protein that shuttles between the nucleus and cytoplasm. Ssd1 interacts with its target mRNAs initially during transcription by binding through its N-terminal prion-like domain (PLD) to the C-terminal domain of RNA polymerase II. Ssd1 subsequently targets mRNAs acquired in the nucleus either to daughter cells for translation or to stress granules (SGs) and P-bodies (PBs) for mRNA storage or decay. Here we show that PB components assist in the nuclear export of Ssd1and subsequent targeting of Ssd1 to PB sites in the cytoplasm. In the absence of import into the nucleus, Ssd1 fails to associate with PBs in the cytoplasm but rather is targeted to cytosolic insoluble protein deposits (IPODs). The association of Ssd1 either with IPOD sites or with PB/SG requires the PLD, whose activity is differentially regulated by the Ndr/LATS family kinase, Cbk1: phosphorylation suppresses PB/SG association but enhances IPOD formation. This regulation likely accrues from a phosphorylation-sensitive nuclear localization sequence located in the PLD. The results presented here may inform our understanding of aggregate formation by RBP in certain neurological diseases.**

Monitoring Editor
Susan Strome
University of California, Santa Cruz

Received: Feb 10, 2017
Revised: Aug 8, 2017
Accepted: Aug 30, 2017

INTRODUCTION

Many proteins in the eukaryotic cell are targeted to specific subcellular compartments, and this targeting is often critical for the execution of the proteins' functions and for survival of the cell. Organelles, such as mitochondria, Golgi, and secretory vesicles, are separated from the cytoplasm by a closed intracellular membrane. However, other distinct cellular structures are not bounded by membranes but comprise specific cytoplasmic complexes of discrete proteins and RNAs. The best studied of these are processing bodies, or P-bodies (PBs), and stress granules (SGs) (Anderson and Kedersha, 2009; Decker and Parker, 2012).

PBs are conserved from yeast to mammals and contain a core of proteins consisting of the mRNA decapping machinery, including the decapping enzyme Dcp1/Dcp2 and the activators of decapping Dhh1, Scd6, and Edc3, as well as mRNAs (Eulalio *et al.*, 2007; Decker and Parker, 2012; Jain and Parker, 2013). These components function in both translation repression and mRNA degradation and compete with the assembly of translational factors (Bhattacharyya *et al.*, 2006; Buchan, 2014). PBs are present in cells during normal growth but increase in number in cells subjected to stress, such as nutrient deprivation, heat shock, or other events that lead to a reduction in translation initiation. SGs are present only in cells subjected to stress or in which translational initiation has been abrogated. Their composition overlaps that of PBs but in addition includes translation initiation factors, poly(A) RBP, and the 40S ribosomal subunit (Decker and Parker, 2012).

Both PBs and SGs are dynamic structures whose components rapidly exchange with their cytoplasmic counterparts. Recent evidence suggests that they may be liquid phase droplets that

This article was published online ahead of print in MBoC in Press (http://www.molbiolcell.org/cgi/doi/10.1091/mbc.E17-02-0100) on September 6, 2017.

[†]Present address: Brain and Mind Research Institute, Weill Cornell Medicine, 413 E. 69th St., New York, NY 10065.

*Address correspondence to: Cornelia Kurischko (cmk2008@med.cornell.edu).

Abbreviations used: aa, amino acids; ALS, amyotrophic lateral sclerosis; CytoQ, cytoplasmic Q-bodies; INQ/JUNQ, intranuclear/juxtanuclear quality control compartments; IPOD, insoluble protein deposition site; NES, nuclear export sequence; NLS, nuclear localization sequence; PBs, P-bodies; pCTD of pol II, Ser2/Ser5 phosphorylated C-terminal domain of RNA polymerase II; PLD, prion-like domain; RBD, RNA-binding domain; RBP, RNA-binding protein; RNP, ribonucleoprotein; SGs, stress granules.

© 2017 Kurischko and Broach. This article is distributed by The American Society for Cell Biology under license from the author(s). Two months after publication it is available to the public under an Attribution–Noncommercial–Share Alike 3.0 Unported Creative Commons License (http://creativecommons.org/licenses/by-nc-sa/3.0).

"ASCB®," "The American Society for Cell Biology®," and "Molecular Biology of the Cell®" are registered trademarks of The American Society for Cell Biology.

form as a result of a phase transition process driven by weak multivalent interactions among the components of the aggregates (Weber and Brangwynne, 2012). Both low complexity sequences, such as prion-like domains (PLDs), and RNA components of these aggregates contribute to the multivalent interactions, and the nature and extent of these components can dictate the location and physical properties of the aggregates (Guo and Shorter, 2015; Zhang *et al.*, 2015). Consistent with this observation, RNA-binding proteins (RBPs) comprise a significant proportion of these aggregates and such proteins often encompass a PLD. Moreover, a disproportionate number of such RBPs are associated with pathogenic aggregates in a variety of neurodegenerative diseases, such as amyotrophic lateral sclerosis (ALS) and Parkinson's disease (Ramaswami *et al.*, 2013).

More recent observations have added to the number of distinct nonmembrane bound cytoplasmic compartments. Narayanaswamy *et al.* (2009) showed that a large fraction of normally soluble metabolic enzymes in *Saccharomyces cerevisiae* forms discrete aggregates in the cytoplasm upon nitrogen starvation, and Shah *et al.* (2014) showed that a significant number of kinases in *Saccharomyces* form cytoplasmic aggregates upon transition into stationary phase. Some of these aggregates overlap with PBs and SGs, but others comprise different distinct foci. Like SGs, these aggregates disperse upon the cells' return to normal growth.

Although the nonmembrane bounded cytoplasmic compartments described above serve at least in part as transitory storage sites for mRNAs and proteins to be reused after cessation of stress, several discrete sites serve as cellular deposition sites for misfolded proteins that arise from proteotoxic stress. In *Saccharomyces cerevisiae*, several such sequestration sites exist: insoluble protein deposits (IPODs), intranuclear or juxtanuclear quality control compartments (INQs/JUNQs), and aggresomes and cytoplasmic Q-bodies (CytoQs) (Kaganovich *et al.*, 2008; Wang *et al.*, 2009; Miller *et al.*, 2015; Sin and Nollen, 2015). They are distinguished by their location in the cell, with IPODs located adjacent to the vacuole, INQs in the nucleus adjacent to the nucleolus, and CytoQs as dispersed aggregates in the cytoplasm. The sites are also distinguished by the type of misfolded proteins and the specific chaperones associated with them. For instance, IPODs preferentially form from amyloidogenic proteins, such as prions, and recruit the chaperone system consisting of the Hsp70 member, Hsp104, and specifically the Hsp40 member, Sis1 (Miller *et al.*, 2015). Aggresomes are specific sites at the spindle pole body, forming only upon expression of human huntingtin exon 1 with an expanded polyglutamine domain. What targets RBPs to their deposition sites versus the ribonucleoprotein (RNP) granules described above is not clear. Here we show that nuclear import and PLD phosphorylation combine to specify to which cytoplasmic particle the yeast RBP Ssd1 localizes.

Ssd1 is a nucleocytoplasmic shuttling protein with multiple functions in the life cycle of its bound mRNAs, particularly those that are destined for polarized localization and translation (Kurischko *et al.*, 2011b). Ssd1 contains a single canonical nuclear localization signal (NLS), and once Ssd1 enters the nucleus it binds through its RNA-binding domain (RBD) to a set of ~50 mRNAs, a majority of which encode cell wall proteins. Ssd1 exports these mRNAs out of the nucleus and delivers them to sites of polarized growth (Figure 1A; Uesono *et al.*, 1997; Hogan *et al.*, 2008; Jansen *et al.*, 2009; Kurischko *et al.*, 2011a,b; Mitchell *et al.*, 2013). Upon stress, Ssd1 and its bound mRNAs localize to SGs and PBs likely through direct interaction between Ssd1 and components of PBs and SGs (Tarassov *et al.*, 2008; Kurischko *et al.*, 2011a; Richardson *et al.*, 2012; Zhang *et al.*, 2014). Ssd1 is the essential substrate of Cbk1, a highly conserved tumor suppressor Ndr/LATS kinase. Deletion of *CBK1* or elimination of the phosphorylation sites on Ssd1 targets it and its bound mRNAs irreversibly to PBs and is lethal (Jansen *et al.*, 2009; Kurischko *et al.*, 2011a). Here we show that PB/SG components play a role in the nuclear export of Ssd1, indicating that interaction between Ssd1 and PB components occurs initially in the nucleus. Moreover, in the absence of association with these components in the nucleus, Ssd1 is targeted to IPODs. Both the association with PB/SG and with IPODs requires the N-terminal PLDs and these associations are inversely affected by Ssd1's phosphorylation status (Figure 1B). Similar processes may contribute to aggregate formation of RBPs in certain neurological diseases such as ALS (Ramaswami *et al.*, 2013).

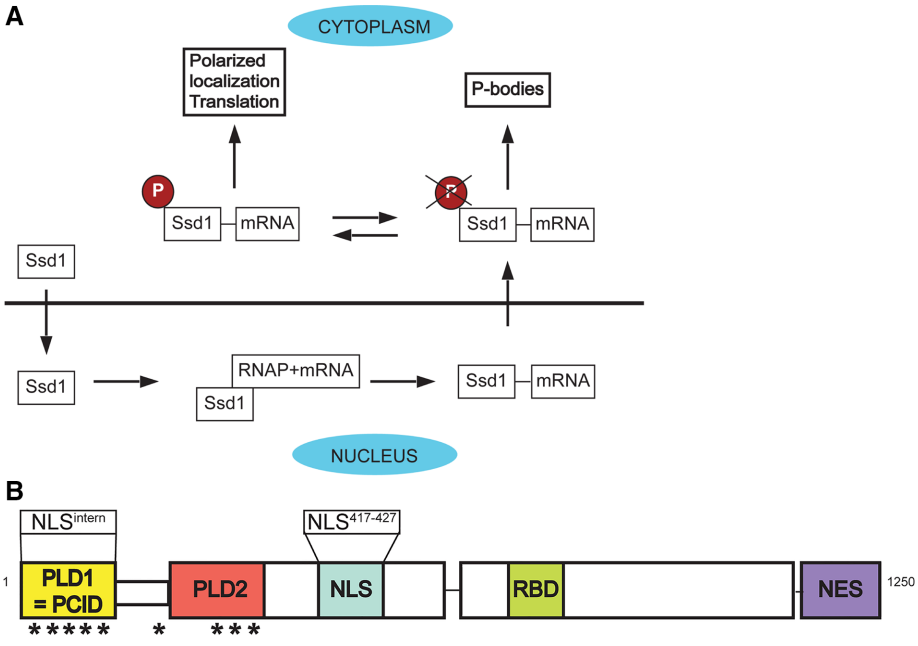

FIGURE 1: Ssd1 function and structure. (A) Ssd1 enters the nucleus by means of its canonical NLS to cotranscriptionally bind its target RNAs. In the cytoplasm it either transports the mRNAs for polarized translation (phosphorylated Ssd1) or associates with PB/SG for mRNA storage or decay (dephosphorylated Ssd1). The cartoon represents a summary of previously published data (Phatnani *et al.*, 2004; Kurischko *et al.*, 2011b). (B) The N-terminus of Ssd1 carries two PLDs, PLD1 (aa 1–162) and PLD2 (aa 263–336). PLD1 corresponds to the previously described PolII C-terminus interacting domain (PCID) (Phatnani *et al.*, 2004) and, as described in this report, also contains a noncanonical nuclear localization sequence (NLS^{intern}). Other domains carry an NLS at amino acids 417–427 ($NLS^{417–427}$), an RNA-binding domain (RBD), and a nuclear export signal (NES). Stars indicate sites of phosphorylation by the Cbk1 kinase (Kurischko *et al.*, 2011a,b).

RESULTS

P-body and stress granule localization of yeast Ssd1 depends on its PLDs

PLDs potentiate protein–protein interactions often as a means of directing proteins to their appropriate functional sites within a cell (Hennig *et al.*, 2015; March *et al.*, 2016).

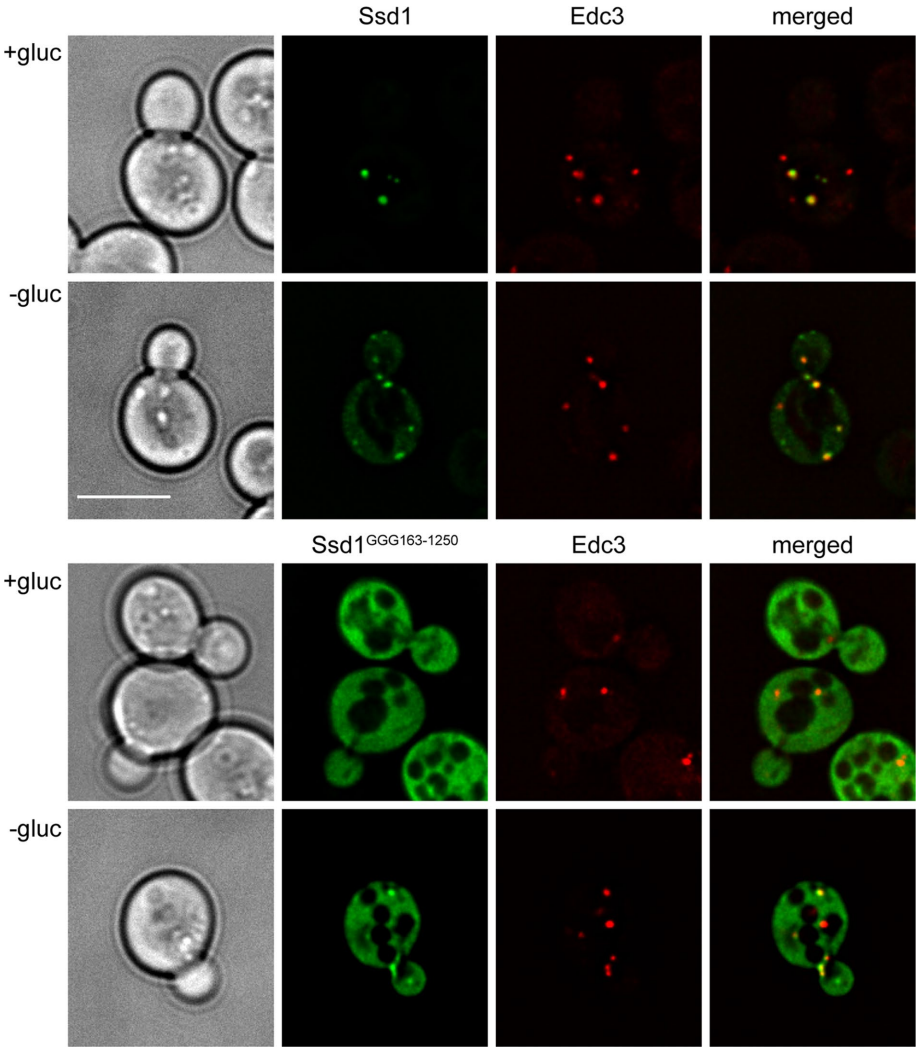

FIGURE 2: Ssd1 PLDs are required for Ssd1 association with PBs. Fluorescence micrographs of strain FLY2184 (*ssd1*Δ) harboring CEN ARS plasmids carrying pRP1574 (YCp-*EDC3*-RFP) and either FLE1019 (pAG415-P_{GPD1}-*SSD1*-GFP; top panels) or B3053 (pAG415-P_{GPD1}-*SSD1*$^{GGG163–1250}$-GFP; bottom panels). Images were taken of cells growing in SC-Leu-Ura+2% glucose (+gluc) or 12 min following a shift to SC-Leu-Ura lacking glucose (-gluc). Bar, 5 μm.

The N-terminus of Ssd1 carries several potential PLDs, as determined by a hidden Markov model for predicting prions (Figure 1B; Alberti *et al.*, 2009). Two of these, aa 1–23 and aa 48–154, are nearly contiguous and we consider this a single domain and refer to aa 1–162 as PLD1. PLD1 corresponds to the domain that binds the phosphorylated C-terminal domain of RNA polymerase II (Phatnani *et al.*, 2004). A second potential PLD is predicted for aa 263–336. All but one (S228) Cbk1 phosphorylation sites in Ssd1 lie in these two PLDs (Mazanka *et al.*, 2008; Jansen *et al.*, 2009) and dephosphorylation of these sites results in constitutive PB association of Ssd1 (Kurischko *et al.*, 2011a). To determine whether either or both PLDs are required for association of Ssd1 with PBs and/or SGs, we constructed Ssd1 variants deleted for aa 1–162 and aa 1–331, accordingly. Because Ssd1$^{163–1250}$-GFP and Ssd1$^{332–1250}$-GFP proteins expose an unfavorable N-terminal amino acid and are highly unstable in the cell (Bachmair *et al.*, 1986), we inserted three glycine residues at the N-termini (Ssd1$^{GGG163–1250}$, Ssd1$^{GGG332–1250}$), which stabilized the proteins. As previously reported, a portion of wild-type Ssd1 protein, expressed under control of the *GPD1* promoter, associated with the PB/SG components even under favorable growth conditions (Kurischko *et al.*, 2011a). We observed that following glucose starvation, essentially all Ssd1 protein formed cytoplasmic foci, many of which colocalized with PB component Edc3 (Figure 2). We then examined the localization of Ssd1 lacking one or both of the PLDs. No cytoplasmic foci were observed for Ssd1$^{GGG163–1250}$-GFP in glucose medium. After shifting cells to glucose-free medium, most of the Ssd1 remained dispersed in the cytoplasm although a few faint foci appeared, but only after longer exposure to glucose deprivation. Some of these foci colocalized or overlapped with Edc3 (Figure 2). P_{GPD1}-*SSD1*$^{GGG332–1250}$-GFP, which lacks both PLDs, showed similar behavior as observed for Ssd1$^{GGG163–1250}$-GFP (Supplemental Figure S1). These experiments document that PLD1 plays a critical role in promoting association of Ssd1 with PBs.

Aggregate formation and nuclear export of Ssd1 require PB components

Kurischko *et al.* (2011a) previously showed that Ssd1 physically associates with PB components. Because certain PB components are crucial for both PB and SG formation, we asked if Ssd1 also depends on them for its association with these structures. Accordingly, we examined the localization of Ssd1 in strains lacking individual PB components. Deletion of *EDC3*, *PAT1* or reduced expression of *NOT1* (DAmP-*not1*) eliminates Ssd1 cytoplasmic foci formation although PBs form, albeit at a reduced rate, in *edc3*Δ and *pat1*Δ strains (Figure 3A; Decker *et al.*, 2007; Teixeira and Parker, 2007). In addition, Ssd1 fails to form foci in cells lacking the SG component Pbp1. However, Ssd1 foci formation occurs normally in cells lacking the SG component Pub1 (Figure 3B). This indicates that association of Ssd1 with a PB requires the presence of several PBs and some SG components. Furthermore, as is evident from Figure 3A, Ssd1 in a wild-type background exhibits no detectable accumulation in the nucleus, but in those strains in which Ssd1 fails to form foci, a significant fraction of the protein resides in the nucleus. Thus cytoplasmic foci formation correlates with export from the nucleus. Although this correlation might point to a requirement for functional PBs or SGs to provide a sink to trap Ssd1 in the cytoplasm and thus extract it from the nuclei, a more compelling interpretation is that PB components associate with Ssd1 in the nucleus to facilitate its nuclear export and target it for cytoplasmic PB granules. Consistent with this hypothesis, Pat1, Not1, and Pbp1 are nucleocytoplasmic shuttling proteins (Collart and Struhl, 1994; Kumar *et al.*, 2002; Haimovich *et al.*, 2013b). Thus we surmise that at least three PB components and one SG protein likely facilitate Ssd1's transport out of the nucleus.

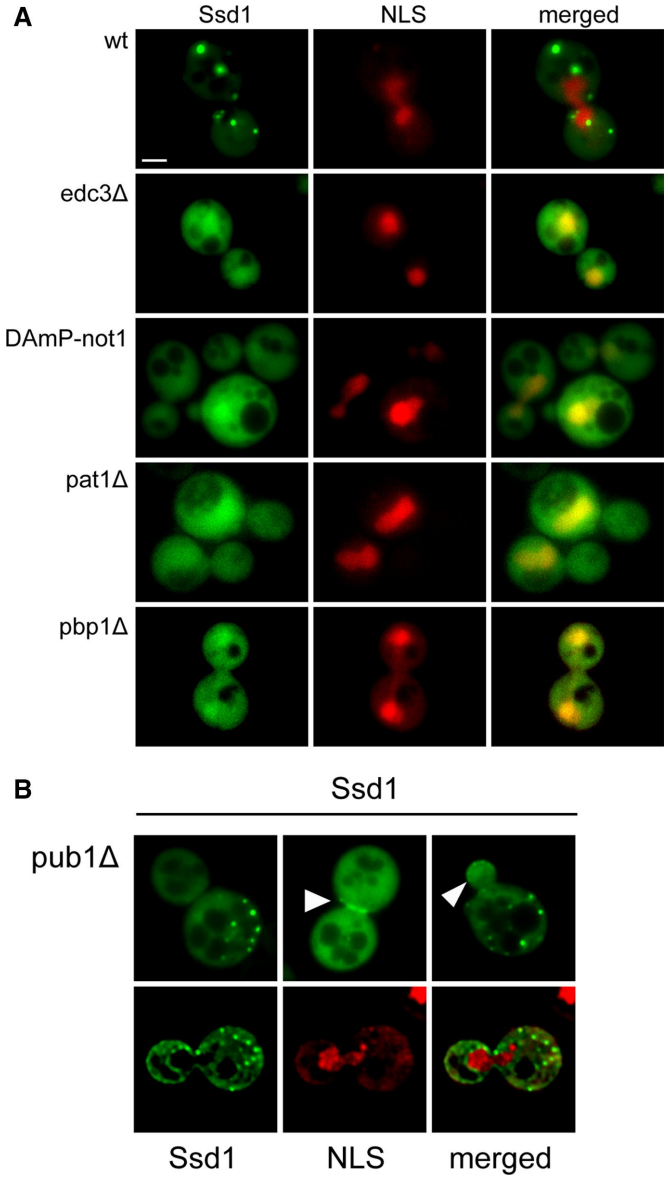

FIGURE 3: Aggregate formation and nuclear export of Ssd1 require PB components but not all SG components. (A) Fluorescence micrographs of strains FLY2184 ("wt"), BY4741 *edc3*Δ ("edc3Δ"), BY4741 *not1*::DAmP-*NOT1* ("DAmP-not1"), BY4741 *pat1*Δ ("pat1Δ"), and BY4741 *pbp1*Δ ("pbp1Δ") harboring plasmids FLE1019 (pAG415-P_{GPD1}-*SSD1*-GFP) and B3070 (pRS426-NLS-RFP) grown on SC+2% glucose lacking leucine and uracil. Bar, 2 µm. (B) Fluorescence micrographs were taken of strain BY4741 *pub1*Δ ("pub1Δ") harboring plasmids FLE1019 (pAG415-P_{GPD1}-*SSD1*-GFP) and, bottom panel only, B3070 (pRS426-NLS-RFP) grown on SC+2% glucose lacking leucine and uracil. Arrowheads indicate bud neck and bud cortex localization of Ssd1-GFP.

Cytoplasmically restricted Ssd1 forms IPODs

Kurischko *et al.* (2011b) previously identified a single NLS within Ssd1 located at amino acids 417–427. They reported that the mutant protein in which all 11 of these amino acids were converted to alanines, $Ssd1^{(417–427)11A}$, failed to enter the nucleus and accumulated in cytoplasmic aggregates. Although these aggregates colocalized with Edc3, they are morphologically distinct from PBs or SGs (Figure 4; Kurischko *et al.*, 2011b). Besides being larger than PBs and generally presenting as a single aggregate per cell, they often appear as rings or donut shapes. In some cases, they appear honeycombed, perhaps reflecting the compound aggregation of multiple rings. These aggregates form in the absence of PB components (Figure 4), further distinguishing them from PBs as well as from wild-type Ssd1. Rather, these aggregates resemble previously described IPODs.

To investigate whether $Ssd1^{(417–427)11A}$ aggregates comprise IPODs, we examined the colocalization of $Ssd1^{(417–427)11A}$ with Hsp104 and Sis1, a disaggregase and a cooperating protein chaperone that function in protein disaggregation in IPODs. As shown in Figure 5, Hsp104 presents a variety of localization patterns toward $Ssd1^{(417–427)11A}$. Hsp104 either fills the cavity of a $Ssd1^{(417–427)11A}$ ring, surrounds large aggregates, or resides adjacent to smaller foci and rings. In some cases multiple small foci of $Ssd1^{(417–427)11A}$ surround a large "aggregate" of Hsp104 (see also Supplemental Figure S2 and Supplemental Movies S1–S4). Sis1 also localizes to $Ssd1^{(417–427)11A}$ aggregates, either surrounding or permeating them (Figure 5, Supplemental Figure S3, and Supplemental Movies S5–S8). Finally, by staining cells expressing $Ssd1^{(417–427)11A}$-GFP with FM4–64, we determined that these Ssd1 aggregates reside in the cytoplasm adjacent to but outside of vacuoles (Supplemental Figure S4), consistent with the previously reported localization of IPODs (Petroi *et al.*, 2012; Buchan *et al.*, 2013; Tardiff *et al.*, 2013; Miller *et al.*, 2015). In sum, these data are consistent with $Ssd1^{(417–427)11A}$ aggregates as IPODs.

PLD1 of Ssd1 is essential for IPOD formation

Given that IPODs are preferential sites for misfolded and/or amyloid proteins, we asked whether PLDs of Ssd1 are instrumental in forming IPODs. We constructed an Ssd1 variant that combined $NLS^{(417–427)11A}$ with the deletion of PLD1 ($Ssd1^{GGG163–1250,\ (417–427)11A}$-GFP). When expressed from the *GPD1* promoter in an *ssd1*Δ background, this protein localized uniformly in the cytoplasm of cells growing in glucose medium, with no detectable IPOD formation (Figure 6). From these results we conclude that PLD1 of Ssd1 promotes not only its association with PB/SG during stress but also its incorporation into IPODs when restricted to the cytoplasm.

Phosphorylation of PLDs regulates aggregate formation of Ssd1

Phosphorylation has been recently shown to affect the function of some PLDs (Gardiner *et al.*, 2008; Hennig *et al.*, 2015). The N-terminal 336 amino acids of Ssd1 that overlap the PLDs contain nine Cbk1 phosphorylation sites. We assessed the consequence of phosphorylation of Ssd1 on its PB/SG and IPOD formation. We examined the behavior of Ssd1 in which all the phosphorylation sites had been converted to phosphomimetic aspartate residues ($Ssd1^{S/T9D}$). As is evident in Figure 7, this mutant protein shows no PB association or other aggregate formation in unstressed cells, in stark contrast to wild-type Ssd1. However, in conjunction with the NLS mutation, the mutant protein, $Ssd1^{S/T9D,\ (417–427)11A}$, forms IPOD aggregates (Figure 8). Thus we conclude that phosphorylation of the PLD in Ssd1 diminishes PB/SG association of the otherwise wild-type protein but enhances IPOD formation of the cytoplasmically restricted protein.

Dephosphorylated Ssd1, arising either from inactivation of Cbk1 kinase or from elimination of all N-terminal phosphosites ($Ssd1^{S/T9A}$), constitutively localizes to the PB, where it traps mRNAs, and is highly toxic to the cell (Kurischko *et al.*, 2011a). However, while Ssd1 lacking its NLS forms IPODs, we found that such a protein that also lacks the PLD phosphorylation sites fails

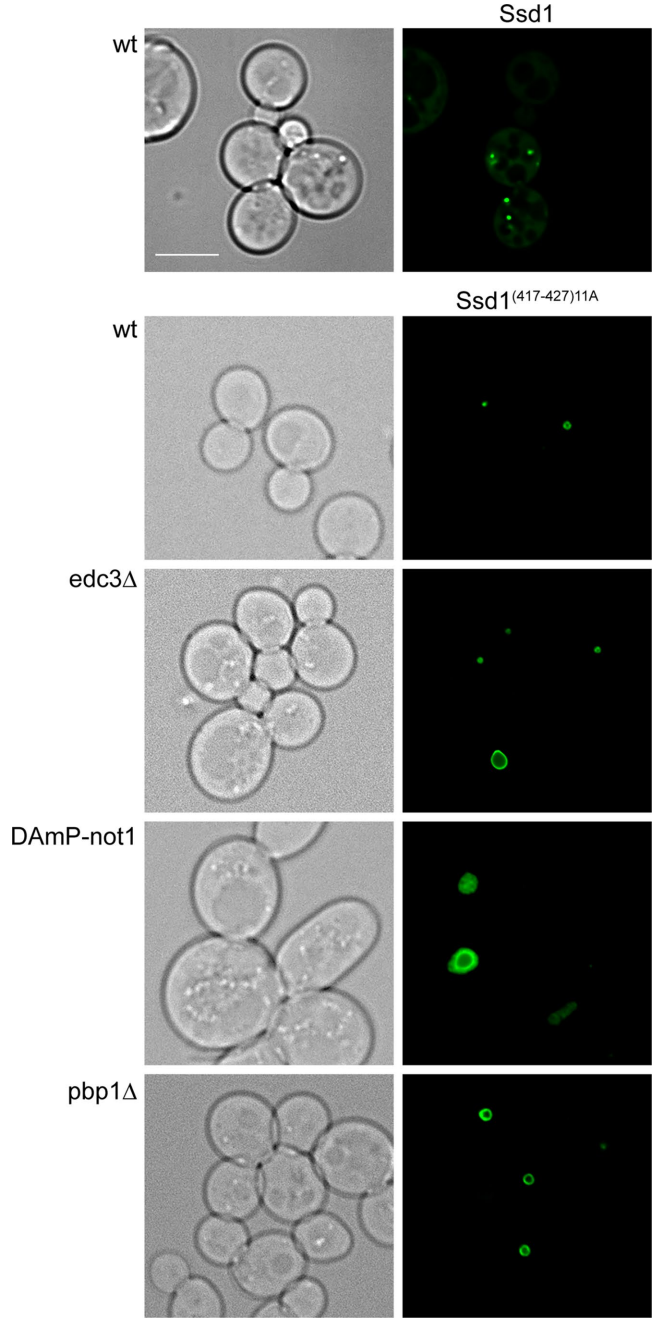

FIGURE 4: Nucleus-excluded Ssd1 localizes to IPOD independently of PB components. Fluorescence micrographs of strain FLY2184 (*ssd1*Δ; "wt") harboring plasmids FLE1019 (pAG415-P_{GPD1}-*SSD1*-GFP) or FLE1213 (pAG415-P_{GPD1}-*ssd1*$^{(417–427)11A}$-GFP) and strains BY4741 *edc3*Δ *SSD1* ("edc3Δ"), BY4741 DAmP-*NOT1 SSD1* ("DAmP-not1"), and BY4741 *pbp1*Δ *SSD1* ("pbp1Δ") harboring plasmid FLE1213. Images were taken of cells growing in SC-Leu+2% glucose. Bar, 5 µm.

to form IPODs and, as shown below, is no longer toxic. Rather, Ssd1$^{S/T9A,\ (417–427)11A}$ forms small uniform aggregates only incidentally coinciding with PB markers (Lsm1, Edc3, and Dcp2) in both unstressed and stressed cells, while significantly overlapping SG markers (Pab1 and Pub1) in nutrient stressed cells (Figure 9, A and B), similar to the behavior of wild-type Ssd1. These observations additionally indicate that Ssd1$^{S/T9A,\ (417–427)11A}$ retains an ability to respond to stress signaling. In sum, we conclude that dephosphorylation of the PLD sites enhances PB/SG localization but prevents IPOD formation in contrast to phosphorylation of the PLD sites, which suppresses PB/SG association but not IPOD formation.

Growth properties of cells with PLD and NLS mutations of *SSD1*

We analyzed the growth properties of cells expressing the various Ssd1 mutants described above (Figure 10, A and B, and Table 1). Cells lacking *SSD1* (*ssd1*Δ) are mildly temperature sensitive and sensitive to the cell wall damaging agent calcofluor white (CFW). Cells carrying a mutant protein lacking a functional NLS (*ssd1*$^{(417–427)11A}$) as the sole copy of the gene show the same phenotype, indicating that the NLS mutant fails to complement the deletion (Figure 10A). However, this mutant protein is not simply nonfunctional because its overexpression inhibits cell growth (Figure 10B), perhaps as a consequence of aggregate formation. The fact that deletion of PLD1 from the NLS mutant protein (Ssd1$^{GGG163–1250,(417–427)11A}$) prevents aggregate formation, but only partially suppresses the overexpression growth inhibition (Figure 10B), supports the conclusion that both the lack of nuclear functions and aggregate formation contribute to the phenotypes of Ssd1$^{(417–427)11A}$. Interestingly, the deletion of one or both PLDs from the otherwise wild-type Ssd1 (Ssd1$^{GGG163–1250}$ and Ssd1$^{GGG336–1250}$) exacerbates the CFW sensitivity and the overexpression toxicity. This observation indicates that the capacity of Ssd1 to associate with PBs fulfills essential functions. Conversion of the phosphosites to phosphomimetic residues combined with mutated NLS (Ssd1$^{S/T9D,(417–427)11A}$) does not alter the phenotypes observed for cells expressing the NLS mutated protein. However, conversion of the phosphosites to nonphosphorylatable residues (Ssd1$^{S/T9A,(417–427)11A}$) completely suppresses the temperature sensitivity and the CFW sensitivity (Figure 10A). Thus the double-mutant protein functions essentially as well as the wild-type protein. This is consistent with the restoration of the subcellular localization properties of the double-mutant protein to those exhibited by the wild-type protein. As previously reported and confirmed here, expression of Ssd1$^{S/T9A}$ completely inhibits cell growth, due apparently to irreversible sequestration of essential mRNAs in PBs or SGs (Kurischko *et al.*, 2011a). This toxicity is partially rescued by the mutated NLS. We conclude that the 9A mutations not only suppress the NLS phenotypes but also that the NLS mutations suppress the 9A phenotypes.

PLD1 contains a phosphorylation-sensitive cryptic NLS

The above results indicate that the absence of N-terminal phosphorylation of Ssd1 suppresses the aggregation phenotype arising from mutation of the protein's NLS. One possible explanation for suppression is that the N-terminal region possesses a phosphorylation-sensitive NLS, such that the protein in its dephosphorylated state could gain entry to the nucleus. To test whether the N-terminal region could facilitate entry into the nucleus, we tagged endogenously expressed Ssd1 after aa 1–200 or aa 1–336 with GFP and analyzed the localization of the protein fragments. As is evident from Figure 11A, these N-terminal fragments are sufficient to localize GFP to the nucleus, demonstrating that a functional NLS resides in the N-terminal domain.

These results demonstrate that the N-terminal domain of Ssd1 (aa 1–200) encompasses a functional NLS, whereas the results obtained with the phosphosite mutants suggest that the activity of this NLS is regulated by Cbk1-mediated phosphorylation. To test this assumption directly, we constructed strains carrying *NIC96*-mCherry as a nuclear marker and in which the only chromosomal copies of

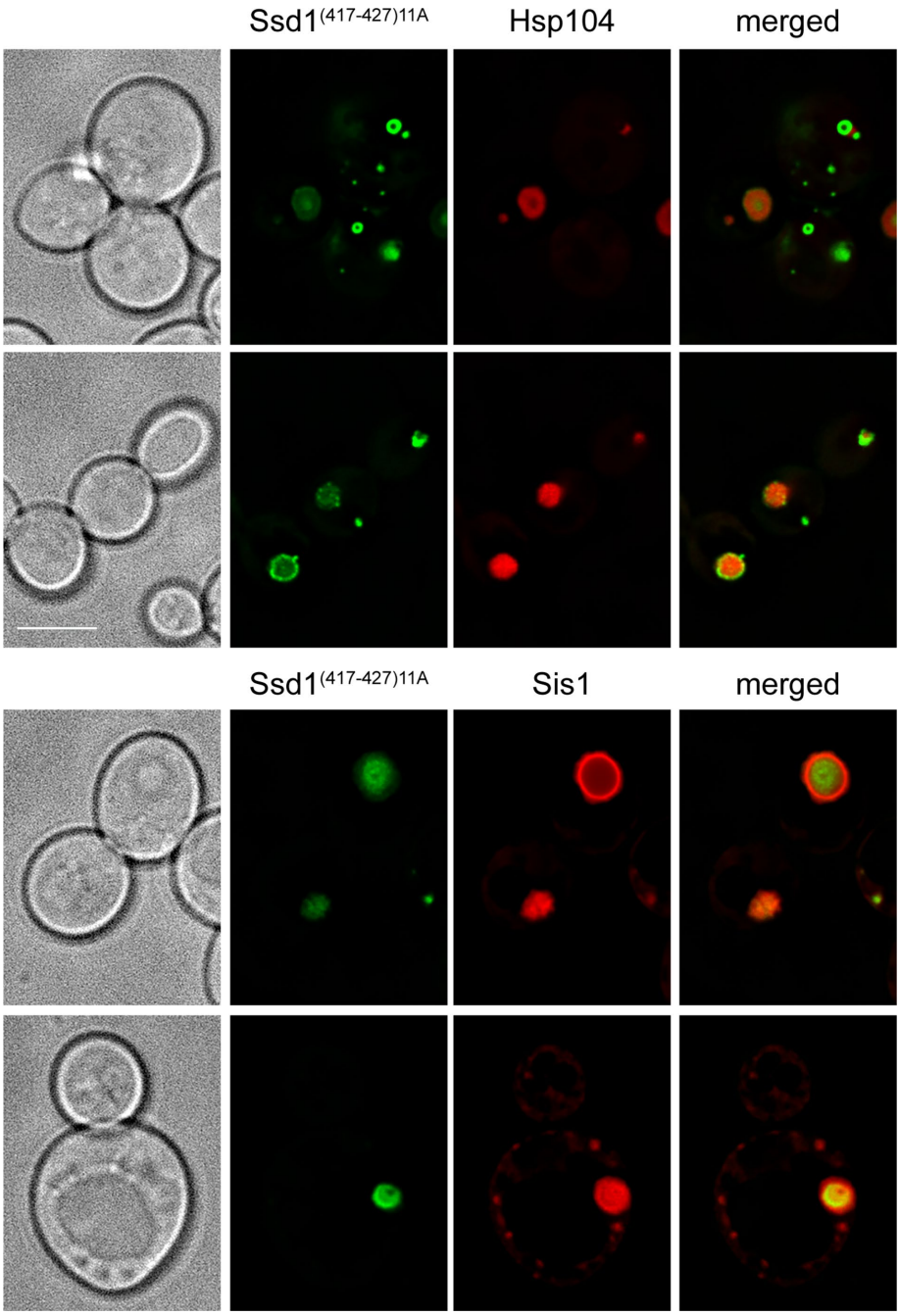

FIGURE 5: Nucleus-excluded Ssd1 colocalizes with IPOD marker proteins. Fluorescence micrographs of strain FLY2184 (*ssd1*Δ) harboring plasmid FLE1213 (pAG415-P_{GPD1}-*ssd1*$^{(417–427)11A}$-GFP) and plasmids O-2189 (*HSP104*-mCherry) or O-2346 (*SIS1*-mCherry). Images were taken of cells growing in SC-Leu-Ura+2% glucose. Single planes from deconvoluted z-stacks are shown. Bar, 5 μm. 3D reconstructions of selected IPODs are shown in Supplemental Figures S3 and S4 and Supplemental Movies S1–S8.

SSD1 are *ssd1*$^{1–200}$-GFP, *ssd1*$^{1–200,\ S5A}$-GFP, or *ssd1*$^{1–200,\ S5D}$-GFP. The nuclear/cytoplasmic ratios of green fluorescent protein (GFP) in these strains confirmed the nuclear accumulation of the *ssd1* N-terminal fragment. Moreover, we observed a significantly reduced level of nuclear accumulation of the N-terminal fragment carrying phosphomimetic variants (S5D), relative to either the wild-type fragment or the nonphosphorylatable fragment (Figure 11B). These results confirm that phosphorylation of the N-terminal domain of Ssd1 reduces its ability to promote nuclear import.

This conclusion gains support from a number of additional observations. First, Kurischko *et al.* (2011b) reported that inhibition of Cbk1 kinase by treating a *cbk1*-as mutant with 1NA-PP1 enhanced the nuclear appearance of the N-terminal Ssd1$^{1–450}$ fragment. Second, nuclear localization of Ssd1 is crucial for suppressing the lethality of *ssd1*Δ *sit4*Δ (Figure 11C): expression of Ssd1 but not Ssd1$^{(417–427)11A}$ is sufficient to support the viability of an *ssd1*Δ *sit4*Δ strain. However, expression of the NLS mutated protein additionally lacking all nine Cbk1 sites (Ssd1$^{S/T9A,\ (417–427)11A}$) does suppress the lethality of the strain. Consistently, conversion of phosphorylation sites to phosphomimetic residues or deletion of PLD1 (Ssd1$^{S/T9D,\ (417–427)11A}$ and Ssd1$^{GGG163–1250,\ (417–427)11A}$) do not suppress the lethality, indicating a requirement for dephosphorylated PLD1 in suppressing the nuclear import defect. Third, Ssd1$^{(417–427)11A}$ fails to fully complement *ssd1*Δ, due to the failure to enter the nucleus to acquire and deliver mRNAs and perhaps as a consequence of IPOD formation. However, Ssd1$^{S/T9A,\ (417–427)11A}$ promotes growth under normal and stressed conditions as well as wild-type Ssd1 (Figure 10). These observations support our hypothesis above that activation of an N-terminal NLS through inhibition of Cbk1-mediated phosphorylation of the protein, by either inactivation of Cbk1 or elimination of its phosphorylation sites, provides an alternate means of importing Ssd1 into the nucleus.

DISCUSSION

Protein trafficking and aggregate formation

Results presented here demonstrate that Ssd1 can reside in three distinct cytoplasmic compartments: uniformly dispersed throughout the cytoplasm, incorporated into discrete P-body or stress granule aggregates, or targeted for degradation/recycling in IPOD-like aggregates. Our results also clarify the molecular basis for targeting to the different locales. First, we find that the PLDs of Ssd1 are required for association of Ssd1 with PBs and SGs, consistent with previous observations (Reijns *et al.*, 2008), but in addition, we find that the PLD is required for Ssd1 incorporation into IPOD-like aggregates. Previously described IPODs form around misfolded amyloidogenic proteins Ubc9^{ts}, Rnq1, and Ure2 (Kaganovich *et al.* 2008). A previous study identified the N-terminal region of Ssd1 as a potential PLD but failed to document that this region could form amyloid aggregates (Alberti *et al.*, 2009). This is not inconsistent with our results, because we have shown here that amyloid formation requires phosphorylation of the Ssd1 PLD1 domain, which would not

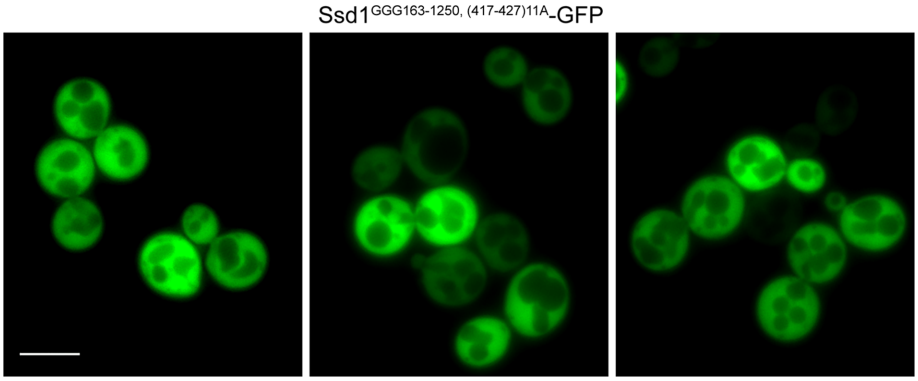

FIGURE 6: PLD1 of Ssd1 is required for IPOD formation. Fluorescence micrographs of strain FLY2184 (*ssd1*Δ) harboring plasmid B3068 (pAG415-P_{GPD1}-*ssd1*$^{GGG163–1250, (417–427)11A}$-GFP). Images were taken of cells growing in SC-Leu+2% glucose. Bar, 5 µm.

have occurred in the previous study. A second aspect of Ssd1 subcellular localization identified here is that nuclear import is required to prevent IPOD formation and promote association of Ssd1 with PB or SG. This suggests that Ssd1 can associate with PB components or mRNAs only within the nucleus and that such initial association in the nucleus is required for subsequent association with PB or SG structures. Moreover, in the absence of nuclear import and subsequent association with mRNAs and/or PB components, Ssd1 forms aggregates that coalesce into IPODs. This may serve as a fail-safe mechanism to ensure that Ssd1 not properly engaged in its normal function is removed from the cytoplasm for recycling or degradation and thereby prevent cellular toxicity. Third, phosphorylation of the PLDs of Ssd1 significantly affects its subcellular localization. Phosphorylation of the domains diminishes association of Ssd1 with PBs/SGs but, in proteins restricted to the cytoplasm, promotes association with IPODs. In contrast, dephosphorylation of these sites enhances association with PB/SG but prevents association of the cytoplasmic restricted protein with IPODs. This could be due to a reduction in the aggregation tendency of the dephosphorylated protein or to activation of the cryptic NLS and restoration of nuclear entry for subsequent acquisition of mRNAs and PB components in the nucleus. The availability of a second NLS, activated upon dephosphorylation during stress, may provide an advantage to the cells. Ssd1 preferentially binds mRNAs encoding cell wall proteins and hence plays a significant role in cell wall integrity. Upon stress, a higher load of mRNAs and their storage in SG may lead to a faster recovery after cessation of the stress conditions.

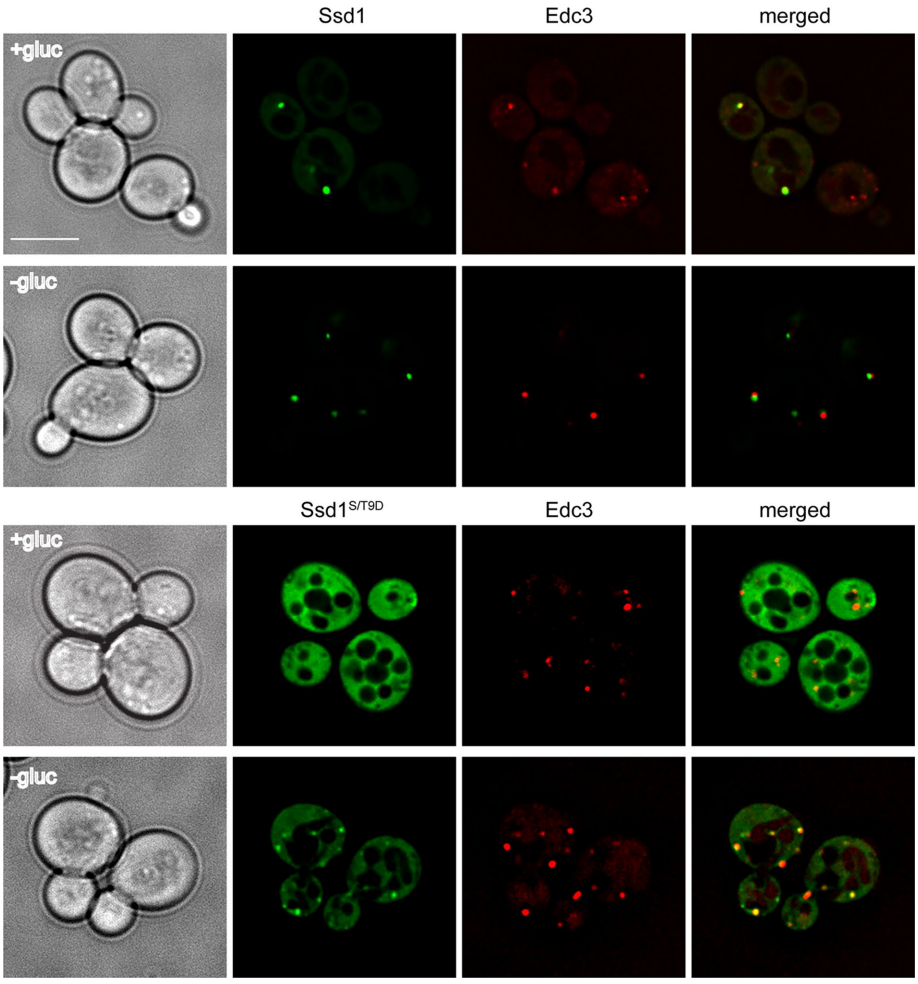

FIGURE 7: Phosphomimetic mutations of Ssd1 diminish association with PBs. Fluorescence micrographs of strain FLY2184 harboring pRP1574 (YCp-*EDC3*-RFP) and either pAG415-P_{GPD1}-*SSD1*-GFP ("Ssd1") or pAG415-P_{GPD1}-*ssd1*$^{S/T9D}$ ("Ssd1$^{S/T9D}$") grown on SC-Leu+2% glucose ("+gluc") or 12 min after a shift to SC-Leu lacking glucose ("-gluc"). Bar, 5 µm.

The nuclear-cytoplasmic cycle of Ssd1

Our studies of Ssd1 functional domains provide insight into the role of nuclear interactions in directing RBPs and their associated mRNAs to their appropriate cytoplasmic location in the cell. Under normal conditions Ssd1 enters the nucleus through the action of its single NLS$^{417–427}$. We suggest that once Ssd1 enters the nucleus, PLDs in the N-terminus of Ssd1 promote its association with pCTD of pol II transcribing certain specific mRNAs. The interaction of Ssd1 with the pCTD would bring Ssd1 into proximity of mRNAs as they are being synthesized, thereby adding an Ssd1-targeted subcellular address to certain mRNAs at the time of initiation of synthesis. Among the mRNAs that Ssd1 binds are those that encode proteins required for cell wall stability and response to cell wall stress, some of which exhibit polarized localization to the daughter cell. This model is consistent with previous data demonstrating an affinity of PLD1 of Ssd1 for the pCTD (Phatnani and Greenleaf, 2004). Moreover, the interaction between RBPs and pCTD of pol II may be a common mechanism for cotranscriptional RNA binding, as was shown for Yra1, a

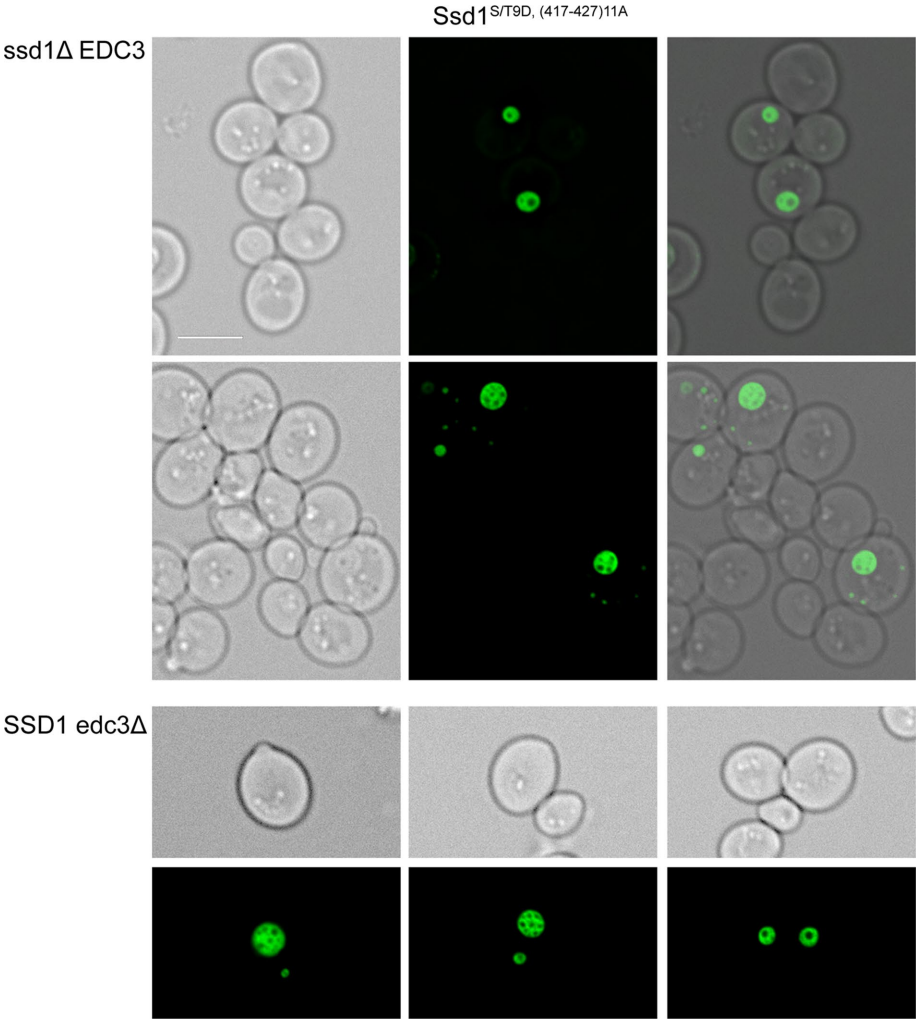

FIGURE 8: Ssd1$^{S/T9D, (417–427)11A}$ exhibits IPOD formation that is independent of Edc3. Fluorescence micrographs of strains FLY2184 ("ssd1Δ EDC3") and BY4741 *edc3*Δ ("SSD1 edc3Δ") harboring B3052 (pAG415-P_{Gal1}-*ssd1*$^{S/T9D, (417–427)11A}$). Images were taken of cells growing on SC-Leu+2% galactose for 2 h.

nuclear poly(A) RNA-binding protein that is required for nuclear export of mRNA (MacKellar and Greenleaf, 2011).

Ssd1 interaction with the pCTD may also promote its association with the PB complex. Recent data have documented that the PB complex interacts with the promoter region of certain genes (Sun *et al.*, 2012; Dahan and Choder, 2013; Haimovich *et al.*, 2013a,b). Thus Ssd1 through its association with pCTD of pol II could engage the PB complex as early as initiation of transcription. Deletion of PLDs eliminates association of Ssd1 with PB even though Ssd1 lacking PLD1 can still bind to PB components (data not shown). This suggests that interaction between Ssd1 and PB components in the nucleus as a consequence of the PLD-mediated association with the pCTD may be a prerequisite for subsequent cytoplasmic localization of Ssd1.

Our results further demonstrate that the interaction of Ssd1 with the components of the mRNA decay machinery in the nucleus are required for efficient export of Ssd1 and subsequent delivery of Ssd1 and its cargo mRNA to the cytoplasm and to PBs and SGs. To the best of our knowledge, this is a novel nuclear role for PB components toward the nuclear export of RBPs. We found that the absence of any of several PB components, the inhibition of Ssd1 nuclear import, or the deletion of regions of the protein required for interaction with pCTD of pol II prevent subsequent association of Ssd1 with PBs. Moreover, the failure of Ssd1 to engage in this process by blocking nuclear import leads to PLD-mediated aggregation of the protein into IPODs, which attract the chaperone complex comprising Hsp104 and the Hsp40 member, Sis1. Thus the interaction of Ssd1 with the PB complex in the nucleus is permissive for subsequent association with PB/SG in the cytoplasm, but presentation of Ssd1 to the complex in the cytoplasm without prior interaction in the nucleus does not lead to productive association. This may simply result from the contribution of mRNA acquired by Ssd1 in the nucleus to the multivalent interactions necessary for liquid phase aggregate formation resulting in PB or SG association. Alternatively, assembly of Ssd1 into PB complex may be an ordered process that is predicated on initial interaction in the nucleus. We summarize the model based on our results in Figure 12.

Ssd1 as a model for neuropathic proteins

The dependency of aggregate formation on PLDs is well documented for human RBPs, such as TDP-43, FUS, and hnRNPA1 (Blokhuis *et al.*, 2013; Kim *et al.*, 2013). We hypothesize that IPODs have similarities with aggregates of FUS and TDP-43 in motor neurons of patients suffering from ALS. The majority of ALS-related mutations in FUS, which promote formation of large cytoplasmic inclusions, occur in its C-terminal NLS. Moreover, deletion of the NLS from FUS in a mouse model leads to aggregate formation (Shelkovnikova *et al.*, 2013a). Although these aggregates contain SG proteins, it is not clear if such structures are related to SGs (Bentmann *et al.*, 2013; Blokhuis *et al.*, 2013). Rather, nuclear import of FUS and its attendant binding to SG proteins may prevent it from association with large aggregates (Shelkovnikova *et al.*, 2013b; Farrawell *et al.*, 2015). By similarity with Ssd1, SG proteins may adhere to large aggregates of mutated FUS or TDP-43, when cells are subjected to stress imposed by the mutated FUS (Farg *et al.*, 2012; Vance *et al.*, 2013). Accordingly, further analysis of the structure-function relationship of Ssd1 could shed light on the pathology of neurotoxic proteins. Moreover, as we see with Ssd1, stimulating alternate trafficking of FUS or TDP-43 might alleviate aggregate formation with attendant therapeutic effect.

MATERIAL AND METHODS

Yeast strains and growth conditions

Standard yeast genetics and culture methods were used (Amberg *et al.*, 2005). For glucose depletion, 1.5 ml of cells was harvested by centrifugation for 30 s and the cell pellet was resuspended in 1 ml glucose-free medium. Cells were incubated for 1 min with

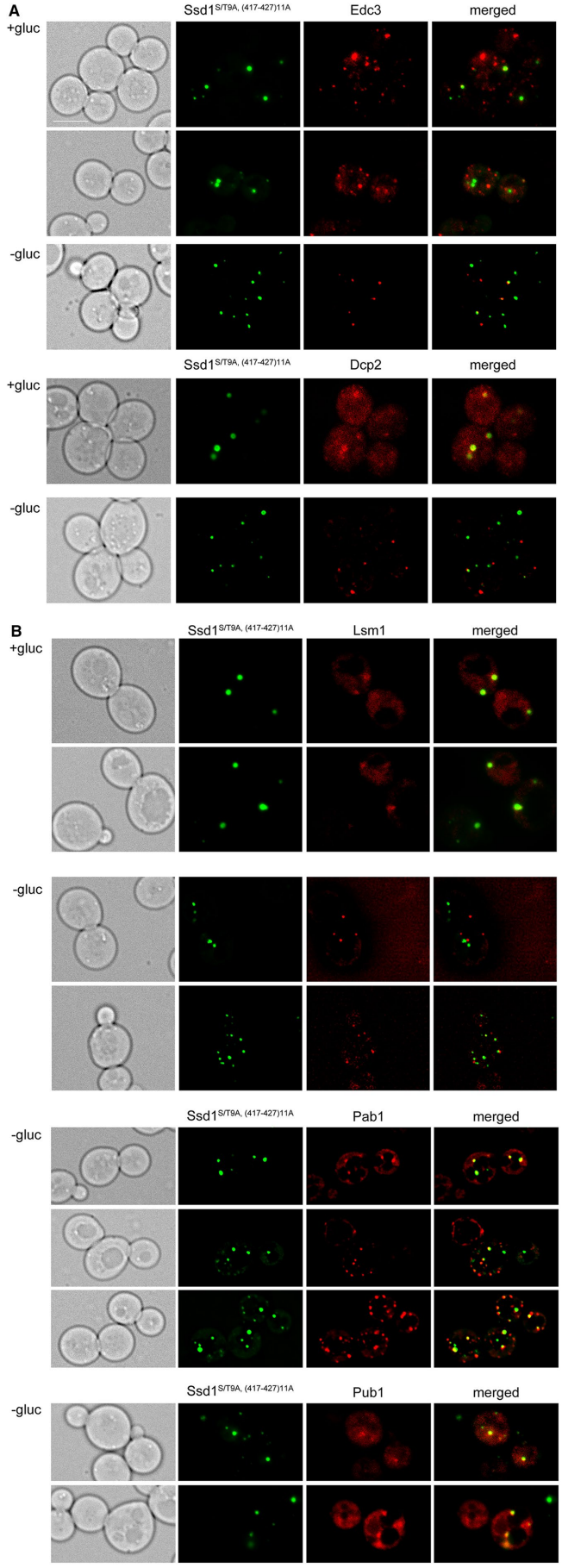

repeated inversion of the Eppendorf tube. Cells were again spun down for 30 s and resuspended in a small volume of the supernatant. Images were taken immediately and over a time course for up to 15 min.

Strain FLY2184 (*MATα his3Δ1 leu2Δ0 met15Δ0 ura3Δ0 ssd1Δ::NATMX*) (Kurischko *et al.*, 2011a) was derived from strain BY4741 (Brachmann *et al.*, 1998) by replacement of the *SSD1* coding region with the NATMX cassette. BY4741-based deletions of *EDC3*, *PAT1*, *PBP1*, and *PUB1* were obtained from the yeast deletion collection. Strain DAmP-*NOT1* was obtained from GE Healthcare Dharmacon. BY4741-based strains with GFP tags inserted after amino acids 200 (Y4183) and 336 (Y4184) of Ssd1 were constructed by transformation with PCR-based cassettes (Longtine *et al.*, 1998). For strains carrying *ssd1*$^{1–200,\ S5A}$*-GFP::KANMX* or *ssd1*$^{1–200,\ S5D}$*-GFP::KANMX* as the only chromosomal copy of SSD1, the NAT cassette of FLY2184 was replaced with the corresponding fragments. These strains were crossed to *Nic96-mCherry::URA3* (Yves Barral, ETH Zurich, Switzerland) to incorporate a nuclear marker. Strain *sit4Δ::KANMX ssd1Δ::NATMX* [B2937] was constructed by crossing single deletion strains and transforming the diploid with B2937 (pRS426-sit4–102) before sporulation and tetrad dissection.

Plasmid construction and molecular biology

PCR fragments of Ssd1$^{GGG163–1250}$ and Ssd1$^{GGG336–1250}$ for Gateway cloning were obtained using the following oligonucleotides:

F for GGG163 5′-GGGGACAAGTTTGTACAAAAAAGCAGGCTTCATGGGTGGT GGTCATTCTTTAGGTCTAAA-3′

F for GGG332 5′-GGGGACAAGTTTGTACAAAAAAGCAGGCTTCATGGGTGGT GGTAATAACGGAGGTGGACG-3′

R for SSD1 5′-GGGGACCACTTTGTACAAGAAAGCTGGGTCTACCCTCTTCATGAATGGATTTAA-3′

pENTRY-Ssd1$^{GGG163–1250}$ and pENTRY-Ssd1$^{GGG336–1250}$ plasmids were constructed by inserting the PCR products into pDONR221 according to the Gateway cloning protocol (Alberti *et al.* 2007).

pENTRY-Ssd1$^{S/T9A,(417–427)11A}$, pENTRY-Ssd1$^{S/T9D,(417–427)11A}$, and pENTRY-Ssd1$^{GGG163–1250,(417–427)11A}$ plasmids were constructed by restriction enzyme–mediated cloning to introduce the NLS$^{(417–427)11A}$ fragment into existing Ssd1$^{S/T9A}$, Ssd1$^{S/T9D}$, and Ssd1$^{GGG163–1250}$ vectors. Tagged Ssd1 variants were constructed by LR Gateway cloning into destination vectors (Alberti *et al.*, 2007).

Plasmids encoding RFP-tagged PB and SG proteins were obtained from Roy Parker (University of Colorado, Boulder) and Charles Cole (Dartmouth Medical School, Hanover, NH). Plasmids carrying *HSP104*-mCherry and *SIS1*-mCherry were provided by S. Alberti,

FIGURE 9: Elimination of Ssd1 phosphorylation prevents IPOD formation of NLS mutant protein. (A) Fluorescence micrographs of strain FLY2184 harboring plasmid B3048 (pAG415-P$_{GPD1}$-*ssd1*$^{S/T9A,(417–427)11A}$-GFP) and a plasmid carrying *DCP2*-RFP, *EDC3*-RFP, or *LSM1*-RFP. Images were taken of cells growing in SC-Leu-Ura+2% glucose ("+gluc") or 1 min after a shift to SC-Leu-Ura lacking glucose ("-gluc"). Ssd1$^{S/T9A,(417–427)11A}$-GFP spots were assessed for their colocalization with PB marker proteins. Bar, 5 μm. (B) Fluorescence micrographs of strain FLY2184 harboring plasmid B3048 (pAG415-P$_{GPD1}$-*ssd1*$^{S/T9A,(417–427)11A}$-GFP) and a plasmid carrying *PAB1*-RFP or *PUB1*-RFP. As Pab1 and Pub1 were not detected in glucose medium, images were taken only of cells in glucose-free medium. Ssd1$^{S/T9A,(417–427)11A}$-GFP spots were assessed for their colocalization with SG marker proteins.

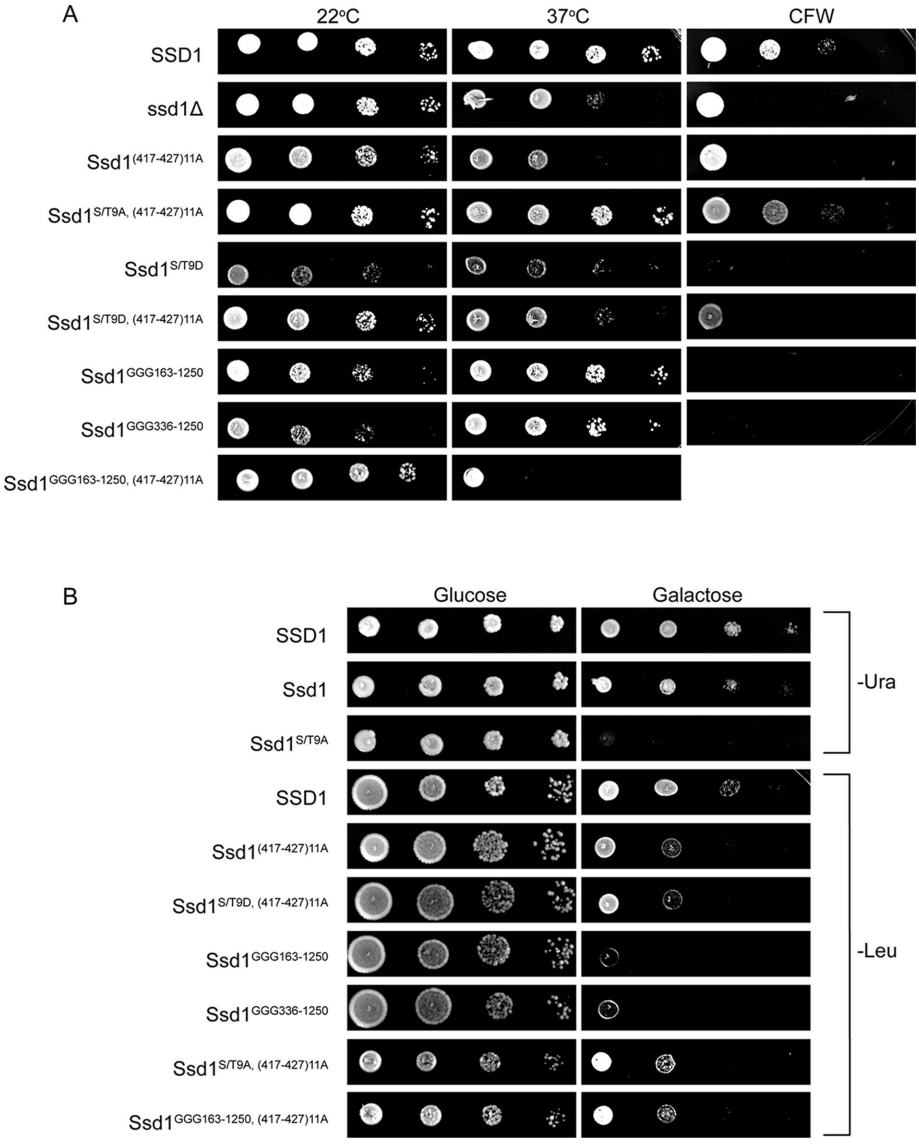

FIGURE 10: Complementary effects of PLD, NLS, and phosphomutations on growth phenotypes of *ssd1* mutant strains.
(A) Growth effects of mutant ssd1 variants expressed from pGPD1. Serial dilutions of the indicated strains spotted on SC-Leu+2% glucose media and imaged after 3 d at RT (22°C) or 37°C as indicated, or on SC-Leu+2% glucose media containing 15 µg/ml calcofluor white (CFW) and imaged after 3 d at RT (22°C). SSD1: BY4741 [pRS415]; ssd1Δ: FLY2184 [pRS415]; Ssd1$^{(417–427)11A}$: FLY2184 [pAG415-P$_{GPD1}$-*ssd1*$^{(417–427)11A}$]; Ssd1$^{S/T9A,(417–427)11A}$: FLY2184 [pAG415-P$_{GPD1}$-*ssd1* $^{S/T9A,(417–427)11A}$]; Ssd1$^{S/T9D}$: FLY2184 [pAG415-P$_{GPD1}$-*ssd1*$^{S/T9D}$]; Ssd1 $^{S/T9D,(417–427)11A}$: FLY2184 [pAG415-P$_{GPD1}$-*ssd1* $^{S/T9D,(417–427)11A}$]; Ssd1$^{GGG163–1250}$: FLY2184 [pAG415-P$_{GPD1}$-*ssd1*$^{GGG163–1250}$]; Ssd1$^{GGG332–1250}$: FLY2184 [pAG415-P$_{GPD1}$-*ssd1*$^{GGG332–1250}$]; Ssd1$^{GGG163–1250,(417–427)11A}$: FLY2184 [pAG415-P$_{GPD1}$-*ssd1*$^{GGG163–1250,(417–427)11A}$]. A summary of all phenotypes is provided in Table 1.
(B) Growth effects of overexpressed mutant ssd1 variants (pGal1). Serial dilutions of the indicated strains spotted on SC+2% glucose or SC+2% galactose media lacking leucine or uracil as indicated and imaged after 3 d at RT (22°C). SSD1: BY4741 [pRS416] or [pRS415]; Ssd1: FLY2184 [pAG416-P$_{GAL1}$-SSD1]; Ssd1$^{S/T9A}$: FLY2184 [pAG416-P$_{GAL1}$-*ssd1*$^{S/T9A}$]; Ssd1$^{(417–427)11A}$: FLY2184 [pAG415-P$_{GAL1}$-*ssd1*$^{(417–427)11A}$]; Ssd1 $^{S/T9D,(417–427)11A}$: FLY2184 [pAG415-P$_{GAL1}$-*ssd1* $^{S/T9D,(417–427)11A}$]; Ssd1$^{GGG163–1250}$: FLY2184 [pAG415-P$_{GAL1}$-*ssd1*$^{GGG163–1250}$]; Ssd1$^{GGG332–1250}$: FLY2184 [pAG415-P$_{GAL1}$-*ssd1*$^{GGG332–1250}$]; Ssd1$^{S/T9A,(417–427)11A}$: FLY2184 [pAG415-P$_{GAL1}$-*ssd1* $^{S/T9A,(417–427)11A}$]; Ssd1$^{GGG332–1250,(417–427)11A}$: FLY2184 [pAG415-P$_{GAL1}$-*ssd1*$^{GGG332–1250,(417–427)11A}$].

	Glucose	Galactose	22°C	37°C	CFW
SSD1	++++	++++	++++	++++	++(+)
ssd1Δ	++++	+++	++++	++	+
[Ssd1] *ssd1Δ*	++++	++(+)	n.d.	n.d.	n.d.
[Ssd1^{PLD1}Δ][a] *ssd1Δ*	++++	+	+++	++++	–
[Ssd1^{PLD1+2}Δ][b] *ssd1Δ*	++++	+	+++	++++	–
[Ssd1^{NLS}Δ][c] *ssd1Δ*	++++	++	++++	++	+
[Ssd1$^{S/T9D}$] *ssd1Δ*	n.d.	n.d.	++++	++++	–
[Ssd1$^{S/T9A}$] *ssd1Δ*	++++	–	–	–	–
[Ssd1$^{S/T9A,NLS}$Δ][d] *ssd1Δ*	++++	++	++++	++++	++(+)
[Ssd1$^{S/T9D,NLS}$Δ][e] *ssd1Δ*	++++	++	++++	++(+)	+
[Ssd1^{PLD1}Δ^{,NLS}Δ][f] *ssd1Δ*	++++	++	++++	++	n.d.

[a]Ssd1$^{GGG163–1250}$.
[b]Ssd1$^{GGG336–1250}$.
[c]Ssd1$^{(417–427)11A}$.
[d]Ssd1$^{S/T9A,(417–427)11A}$.
[e]Ssd1$^{S/T9D,(417–427)11A}$.
[f]Ssd1$^{GGG163–1250,(417–427)11A}$.

TABLE 1: Summary of phenotypes associated with Ssd1 variants.

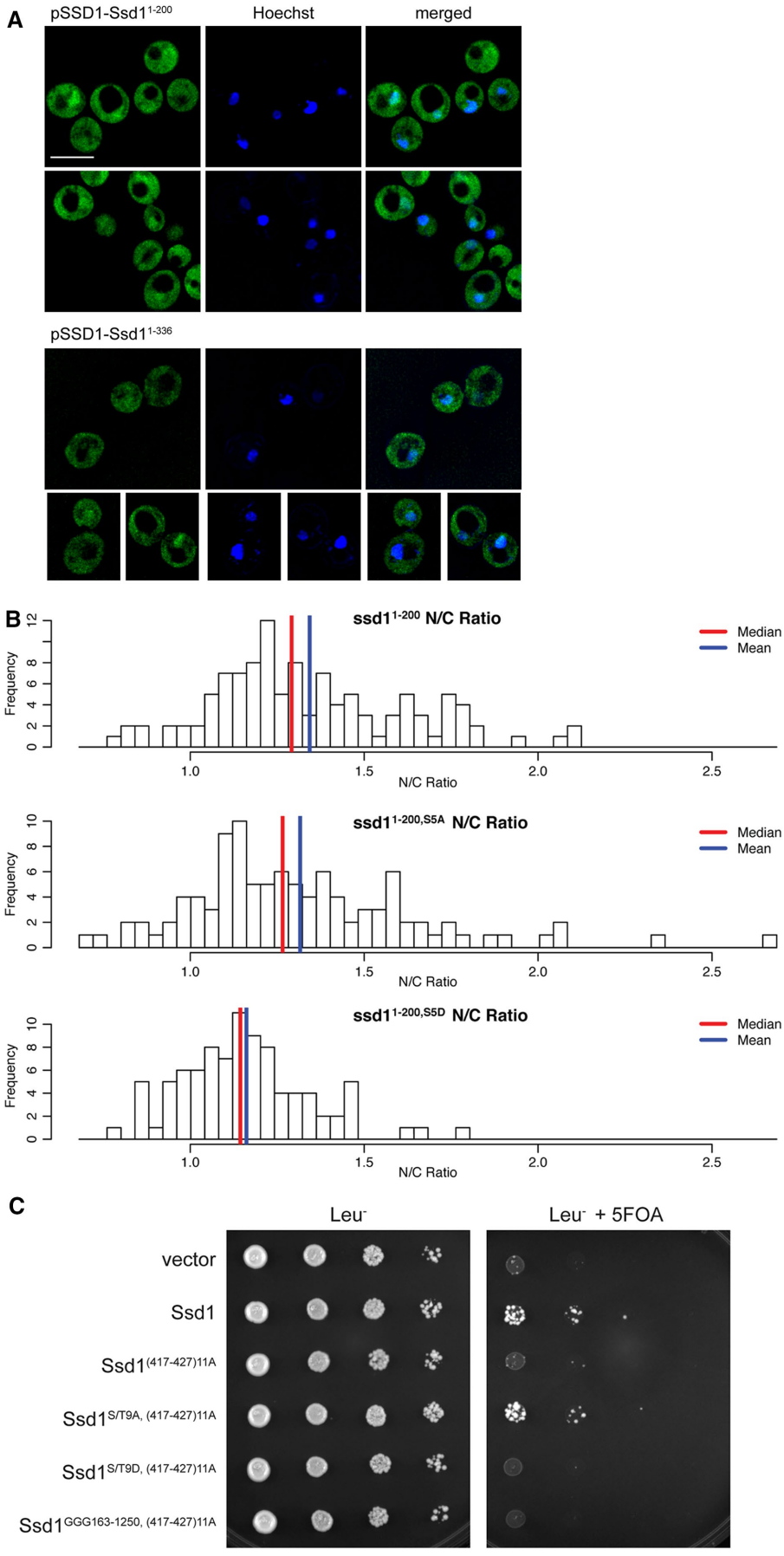

MPI Dresden, Germany. All plasmids are listed in Supplemental Table S1.

Dilution series to define growth capacity

Cell densities of overnight cultures of strains BY4741 [pRS415], BY4741 [pRS416], and ssd1Δ containing the indicated pAG415-P_{Gal1}-*SSD1*-GFP or pAG416-P_{Gal1}-*SSD1*-GFP variants were counted and adjusted to equal numbers of cells/ml. Four microliters of undiluted and serial 10× dilutions was spotted on agar plates containing either 2% glucose or 2% galactose. The plates were incubated for 3 d at 22°C. The same procedure was applied to overnight cultures of strains BY4741 [pRS415], ssd1Δ [pRS415], and ssd1Δ containing the indicated pAG415-P_{GPD1}-*SSD1*-GFP variants. Four microliters of undiluted cultures and 10× dilutions was spotted for growth on SC-Leu at 22°C, SC-Leu at 37°C, and SC-Leu at 22°C with 15 µg/ml CFW agar plates. Images were taken after 3 d. The same protocol was applied for the plasmid shuffle experiment to define the capacity of Ssd1 versions to support the viability of *sit4Δ ssd1Δ* cells.

FIGURE 11: The Ssd1 N-terminal domain encompasses an NLS. (A) Fluorescence micrographs of strain Y4183 in which GFP has been inserted in frame following amino acid 200 ("pSSD1-ssd1$^{1–200}$") or amino acid 336 (strain Y4184, "pSSD1-ssd1$^{1–336}$"), grown on SC-Leu+2% glucose. Nuclei are identified by staining with Hoechst 33342 (Thermo Fisher Scientific). Bar, 5 µm. (B) Nuclear-cytoplasm ratios are presented in histograms for wild-type (ssd1$^{1–200}$), nonphosphorylatable (ssd1$^{1–200,\ S5A}$), and phosphomimetic (ssd1$^{1–200,\ S5D}$) versions of the N-terminal Ssd1 fragment. Both wild-type and S5A differ significantly from S5D, as indicated by *p*-values (9.91e-7 and 4.74e-4, respectively). (C) Viability of *sit4Δ ssd1Δ* cells depends on the nuclear localization of Ssd1. Strain *sit4Δ ssd1Δ* [pRS426-sit4–102] was transformed with pRS415 (vector), FLE1019 (pAG415-P_{GPD1}-*SSD1*-GFP), FLE1213 (pAG415-P_{GPD1}-*ssd1* $^{(417–427)11A}$-GFP), B3048 (pAG415-P_{GPD1}-*ssd1*$^{S/T9A,\ (417–427)11A}$-GFP), B3050 (pAG415-P_{GPD1}-*ssd1*$^{S/T9D,\ (417–427)11A}$-GFP), or B3068 (pAG415-P_{GPD1}-*ssd1*$^{GGG163–1250,\ (417–427)11A}$-GFP). Ten times dilutions were spotted on SC+2% glucose medium without leucine and SC+2% glucose medium without leucine plus 5-fluoroorotic acid (5-FOA) for the counterselection of pRS426-sit4–102. Cells were allowed to grow for 3 and 6 d, respectively.

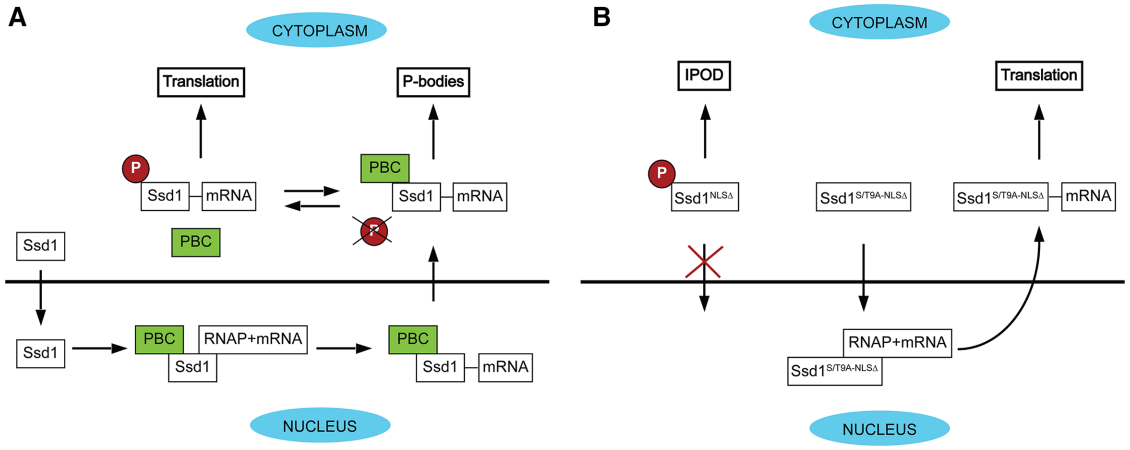

FIGURE 12: Summary of nuclear and cytoplasmic behavior of wild-type Ssd1 and mutated Ssd1$^{(417–427)11A}$. (A) Nuclear events, like association with PB components, and phosphorylation by Cbk1 kinase define the nuclear export and cytoplasmic localization of Ssd1-mRNA complex. (B) Preventing Ssd1 from nuclear localization targets the protein to IPOD. Dephosphorylation of Cbk1 sites restores nuclear localization and prevents IPOD localization. Localization of Ssd1$^{S/T9A,\ (417–427)11A}$ is independent of PBCs. Abbreviations: RNAP, RNA polymerase II; PBC, P-body components.

Deconvolution microscopy

Cells were imaged on a wide-field inverted microscope (DeltaVision; Applied Precision, Issaquah, WA) at Penn State College of Medicine with a charge-coupled device camera (CoolSNAP HQ; Roper Scientific, Tucson, AZ), using a 100× oil-immersion objective, or at Rockefeller University on a DeltaVision Image Restoration Microscope (Olympus IX70 inverted microscope with a pco.edge sCOS camera) using a 100× oil-immersion objective. The percentage transmittance for GFP and RFP channels and the exposure times were individually adjusted to the brightness of the signals, as all signals were plasmid based. Eighteen to twenty 0.2-µm z-stacks were taken of each focal plane using the DeltaVision softWoRx software. Where indicated, deconvolution of the z-stacks was performed. For each strain, at least 50 cells were imaged.

Definition of nuclear-cytoplasmic ratio (N/C)

The fluorescence intensities of individual nuclei and the adjacent cytoplasm were measured by Metamorph software as described previously (Kurischko *et al.*, 2011b). In detail, a defined area in nuclei (N), identified by the nuclear pore marker Nic96-mCherry, was measured in a single plane of deconvolved z-stacks in the GFP channel. The same sized area was measured in the adjacent cytoplasm (C) and outside of cells (background B). The ratios of N-B/C-B were calculated for ~100 nuclei per strain and processed statistically by the Wilcoxon rank sum test.

FM4–64 staining of vacuole membranes

The procedure is a variation of previously published protocol (Vida and Emr, 1995). Five-milliliter cultures were spun down and resuspended in 500 µl YPD. One microliter FM4–64 solution in dimethyl sulfoxide (Molecular Probes Life Technology) was added to a final concentration of 32 µM and incubated in the darkness for 30 min at room temperature (RT). Cells were spun down, washed to remove the excess of FM4–64, and resuspended in synthetic complete growth medium for yeast (SC). Images were taken after 30′ to analyze colocalization of membranes and Ssd1-GFP proteins.

ACKNOWLEDGMENTS

We thank Greg Petsko, in whose laboratory part of this work was conducted, for his ongoing and generous support. We thank Alison North, Kaye Thomas, and Tao Tong of the Bio-Imaging Resource Center of The Rockefeller University, New York, for their assistance in microscopy and image acquisition. We thank Vonn Walter, IPM Penn State University, for statistical analysis. We thank Jacqueline Burre, Weill Cornell Medicine; Susan Liebman, University of Nevada; and Roy Parker, University of Colorado, for helpful discussions and suggestions for the manuscript. This work was supported by National Institutes of Health grant GM076562 to J.R.B. and in part under a grant with the Pennsylvania Department of Health using Tobacco CURE funds. The Department specifically disclaims responsibility for any analyses, interpretations, or conclusions.

REFERENCES

Alberti S, Gitler AD, Lindquist S (2007). A suite of Gateway cloning vectors for high-throughput genetic analysis in *Saccharomyces cerevisiae*. Yeast 24, 913–919.

Alberti S, Halfmann R, King O, Kapila A, Lindquist S (2009). A systematic survey identifies prions and illuminates sequence features of prionogenic proteins. Cell 137, 146–158.

Amberg DC, Burke DJ, Strathern JN (2005). Methods in Yeast Genetics: A Cold Spring Harbor Laboratory Course Manual, 2005 ed., Cold Spring Harbor, NY: Cold Spring Harbor Laboratory Press.

Anderson P, Kedersha N (2009). RNA granules: post-transcriptional and epigenetic modulators of gene expression. Nat Rev Mol Cell Biol 10, 430–436.

Bachmair A, Finley D, Varshavsky A (1986). In vivo half-life of a protein is a function of its amino-terminal residue. Science 234, 179–186.

Bentmann E, Haass C, Dormann D (2013). Stress granules in neurodegeneration—lessons learnt from TAR DNA binding protein of 43 kDa and fused in sarcoma. FEBS J 280, 4348–4370.

Bhattacharyya SN, Habermacher R, Martine U, Closs EI, Filipowicz W (2006). Stress-induced reversal of microRNA repression and mRNA P-body localization in human cells. Cold Spring Harb Symp Quant Biol 71, 513–521.

Blokhuis AM, Groen EJ, Koppers M, van den Berg LH, Pasterkamp RJ (2013). Protein aggregation in amyotrophic lateral sclerosis. Acta Neuropathol 125, 777–794.

Brachmann CB, Davies A, Cost GJ, Caputo E, Li J, Hieter P, Boeke JD (1998). Designer deletion strains derived from *Saccharomyces cerevisiae* S288C: a useful set of strains and plasmids for PCR-mediated gene disruption and other applications. Yeast 14, 115–132.

Buchan JR (2014). mRNP granules. Assembly, function, and connections with disease. RNA Biol 11, 1019–1030.

Buchan JR, Kolaitis RM, Taylor JP, Parker R (2013). Eukaryotic stress granules are cleared by autophagy and Cdc48/VCP function. Cell 153, 1461–1474.

Collart MA, Struhl K (1994). NOT1(CDC39), NOT2(CDC36), NOT3, and NOT4 encode a global-negative regulator of transcription that differentially affects TATA-element utilization. Genes Dev 8, 525–537.

Dahan N, Choder M (2013). The eukaryotic transcriptional machinery regulates mRNA translation and decay in the cytoplasm. Biochim Biophys Acta 1829, 169–173.
Decker CJ, Parker R (2012). P-bodies and stress granules: possible roles in the control of translation and mRNA degradation. Cold Spring Harb Perspect Biol 4, a012286.
Decker CJ, Teixeira D, Parker R (2007). Edc3p and a glutamine/asparagine-rich domain of Lsm4p function in processing body assembly in *Saccharomyces cerevisiae*. J Cell Biol 179, 437–449.
Eulalio A, Behm-Ansmant I, Schweizer D, Izaurralde E (2007). P-body formation is a consequence, not the cause, of RNA-mediated gene silencing. Mol Cell Biol 27, 3970–3981.
Farg MA, Soo KY, Walker AK, Pham H, Orian J, Horne MK, Warraich ST, Williams KL, Blair IP, Atkin JD (2012). Mutant FUS induces endoplasmic reticulum stress in amyotrophic lateral sclerosis and interacts with protein disulfide-isomerase. Neurobiol Aging 33, 2855–2868.
Farrawell NE, Lambert-Smith IA, Warraich ST, Blair IP, Saunders DN, Hatters DM, Yerbury JJ (2015). Distinct partitioning of ALS associated TDP-43, FUS and SOD1 mutants into cellular inclusions. Sci Rep 5, 13416.
Gardiner M, Toth R, Vandermoere F, Morrice NA, Rouse J (2008). Identification and characterization of FUS/TLS as a new target of ATM. Biochem J 415, 297–307.
Guo L, Shorter J (2015). It's raining liquids: RNA tunes viscoelasticity and dynamics of membraneless organelles. Mol Cell 60, 189–192.
Haimovich G, Choder M, Singer RH, Trcek T (2013a). The fate of the messenger is pre-determined: a new model for regulation of gene expression. Biochim Biophys Acta 1829, 643–653.
Haimovich G, Medina DA, Causse SZ, Garber M, Millan-Zambrano G, Barkai O, Chavez S, Perez-Ortin JE, Darzacq X, Choder M (2013b). Gene expression is circular: factors for mRNA degradation also foster mRNA synthesis. Cell 153, 1000–1011.
Hennig S, Kong G, Mannen T, Sadowska A, Kobelke S, Blythe A, Knott GJ, Iyer KS, Ho D, Newcombe EA, *et al.* (2015). Prion-like domains in RNA binding proteins are essential for building subnuclear paraspeckles. J Cell Biol 210, 529–539.
Hogan DJ, Riordan DP, Gerber AP, Herschlag D, Brown PO (2008). Diverse RNA-binding proteins interact with functionally related sets of RNAs, suggesting an extensive regulatory system. PLoS Biol 6, e255.
Jain S, Parker R (2013). The discovery and analysis of P bodies. Adv Exp Med Biol 768, 23–43.
Jansen JM, Wanless AG, Seidel CW, Weiss EL (2009). Cbk1 regulation of the RNA-binding protein Ssd1 integrates cell fate with translational control. Curr Biol 19, 2114–2120.
Kaganovich D, Kopito R, Frydman J (2008). Misfolded proteins partition between two distinct quality control compartments. Nature 454, 1088–1095.
Kim HJ, Kim NC, Wang YD, Scarborough EA, Moore J, Diaz Z, MacLea KS, Freibaum B, Li S, Molliex A, *et al.* (2013). Mutations in prion-like domains in hnRNPA2B1 and hnRNPA1 cause multisystem proteinopathy and ALS. Nature 495, 467–473.
Kumar A, Agarwal S, Heyman JA, Matson S, Heidtman M, Piccirillo S, Umansky L, Drawid A, Jansen R, Liu Y, *et al.* (2002). Subcellular localization of the yeast proteome. Genes Dev 16, 707–719.
Kurischko C, Kim HK, Kuravi VK, Pratzka J, Luca FC (2011a). The yeast Cbk1 kinase regulates mRNA localization via the mRNA-binding protein Ssd1. J Cell Biol 192, 583–598.
Kurischko C, Kuravi VK, Herbert CJ, Luca FC (2011b). Nucleocytoplasmic shuttling of Ssd1 defines the destiny of its bound mRNAs. Mol Microbiol 81, 831–849.
Longtine MS, McKenzie A 3rd, Demarini DJ, Shah NG, Wach A, Brachat A, Philippsen P, Pringle JR (1998). Additional modules for versatile and economical PCR-based gene deletion and modification in *Saccharomyces cerevisiae*. Yeast 14, 953–961.
MacKellar AL, Greenleaf AL (2011). Cotranscriptional association of mRNA export factor Yra1 with C-terminal domain of RNA polymerase II. J Biol Chem 286, 36385–36395.
March ZM, King OD, Shorter J (2016). Prion-like domains as epigenetic regulators, scaffolds for subcellular organization, and drivers of neurodegenerative disease. Brain Res 1647, 9–18.
Mazanka E, Alexander J, Yeh BJ, Charoenpong P, Lowery DM, Yaffe M, Weiss EL (2008). The NDR/LATS family kinase Cbk1 directly controls transcriptional asymmetry. PLoS Biol 6, e203.
Miller SB, Mogk A, Bukau B (2015). Spatially organized aggregation of misfolded proteins as cellular stress defense strategy. J Mol Biol 427, 1564–1574.
Mitchell SF, Jain S, She M, Parker R (2013). Global analysis of yeast mRNPs. Nat Struct Mol Biol 20, 127–133.
Narayanaswamy R, Levy M, Tsechansky M, Stovall GM, O'Connell JD, Mirrielees J, Ellington AD, Marcotte EM (2009). Widespread reorganization of metabolic enzymes into reversible assemblies upon nutrient starvation. Proc Natl Acad Sci USA 106, 10147–10152.
Petroi D, Popova B, Taheri-Talesh N, Irniger S, Shahpasandzadeh H, Zweckstetter M, Outeiro TF, Braus GH (2012). Aggregate clearance of α-synuclein in *Saccharomyces cerevisiae* depends more on autophagosome and vacuole function than on the proteasome. J Biol Chem 287, 27567–27579.
Phatnani HP, Greenleaf AL (2004). Identifying phosphoCTD-associating proteins. Methods Mol Biol 257, 17–28.
Phatnani HP, Jones JC, Greenleaf AL (2004). Expanding the functional repertoire of CTD kinase I and RNA polymerase II: novel phosphoCTD-associating proteins in the yeast proteome. Biochemistry 43, 15702–15719.
Ramaswami M, Taylor JP, Parker R (2013). Altered ribostasis: RNA-protein granules in degenerative disorders. Cell 154, 727–736.
Reijns MA, Alexander RD, Spiller MP, Beggs JD (2008). A role for Q/N-rich aggregation-prone regions in P-body localization. J Cell Sci 121, 2463–2472.
Richardson R, Denis CL, Zhang C, Nielsen MEO, Chiang YC, Kierkegaard M, Wang X, Lee DJ, Andersen JS, Yao G (2012). Mass spectrometric identification of proteins that interact through specific domains of the poly(A) binding protein. Mol Genet Genomics 287, 711–730.
Shah KH, Nostramo R, Zhang B, Varia SN, Klett BM, Herman PK (2014). Protein kinases are associated with multiple, distinct cytoplasmic granules in quiescent yeast cells. Genetics 198, 1495–1512.
Shelkovnikova TA, Peters OM, Deykin AV, Connor-Robson N, Robinson H, Ustyugov AA, Bachurin SO, Ermolkevich TG, Goldman IL, Sadchikova ER, *et al.* (2013a). Fused in sarcoma (FUS) protein lacking nuclear localization signal (NLS) and major RNA binding motifs triggers proteinopathy and severe motor phenotype in transgenic mice. J Biol Chem 288, 25266–25274.
Shelkovnikova TA, Robinson HK, Connor-Robson N, Buchman VL (2013b). Recruitment into stress granules prevents irreversible aggregation of FUS protein mislocalized to the cytoplasm. Cell Cycle 12, 3194–3202.
Sin O, Nollen EA (2015). Regulation of protein homeostasis in neurodegenerative diseases: the role of coding and non-coding genes. Cell Mol Life Sci 72, 4027–4047.
Sun M, Schwalb B, Schulz D, Pirkl N, Etzold S, Lariviere L, Maier KC, Seizl M, Tresch A, Cramer P (2012). Comparative dynamic transcriptome analysis (cDTA) reveals mutual feedback between mRNA synthesis and degradation. Genome Res 22, 1350–1359.
Tarassov K, Messier V, Landry CR, Radinovic S, Serna Molina MM, Shames I, Malitskaya Y, Vogel J, Bussey H, Michnick SW (2008). An in vivo map of the yeast protein interactome. Science 320, 1465–1470.
Tardiff DF, Jui NT, Khurana V, Tambe MA, Thompson ML, Chung CY, Kamadurai HB, Kim HT, Lancaster AK, Caldwell KA, *et al.* (2013). Yeast reveal a "druggable" Rsp5/Nedd4 network that ameliorates α-synuclein toxicity in neurons. Science 342, 979–983.
Teixeira D, Parker R (2007). Analysis of P-body assembly in *Saccharomyces cerevisiae*. Mol Biol Cell 18, 2274–2287.
Uesono Y, Toh-e A, Kikuchi Y (1997). Ssd1p of *Saccharomyces cerevisiae* associates with RNA. J Biol Chem 272, 16103–16109.
Vance C, Scotter EL, Nishimura AL, Troakes C, Mitchell JC, Kathe C, Urwin H, Manser C, Miller CC, Hortobagyi T, *et al.* (2013). ALS mutant FUS disrupts nuclear localization and sequesters wild-type FUS within cytoplasmic stress granules. Hum Mol Genet 22, 2676–2688.
Vida TA, Emr SD (1995). A new vital stain for visualizing vacuolar membrane dynamics and endocytosis in yeast. J Cell Biol 128, 779–792.
Wang Y, Meriin AB, Zaarur N, Romanova NV, Chernoff YO, Costello CE, Sherman MY (2009). Abnormal proteins can form aggresome in yeast: aggresome-targeting signals and components of the machinery. FASEB J 23, 451–463.
Weber SC, Brangwynne CP (2012). Getting RNA and protein in phase. Cell 149, 1188–1191.
Zhang H, Elbaum-Garfinkle S, Langdon EM, Taylor N, Occhipinti P, Bridges AA, Brangwynne CP, Gladfelter AS (2015). RNA controls polyQ protein phase transitions. Mol Cell 60, 220–230.
Zhang C, Wang X, Park S, Chiang YC, Xi W, Laue TM, Denis CL (2014). Only a subset of the PAB1-mRNP proteome is present in mRNA translation complexes. Protein Sci 23, 1036–1049.